Mohamed Zanaty[1]
Instant-Lab,
École Polytechnique Fédérale de Lausanne,
Neuchâtel 2000, Switzerland
e-mail: mohamed.zanaty@epfl.ch

Thomas Fussinger
Instant-Lab,
École Polytechnique Fédérale de Lausanne,
Neuchâtel 2000, Switzerland
e-mail: thomas.fussinger@epfl.ch

Arno Rogg
Instant-Lab,
École Polytechnique Fédérale de Lausanne,
Neuchâtel 2000, Switzerland
e-mail: arno.rogg@gmail.com

Andrea Lovera
FEMTOprint SA,
Muzzano 6933, Switzerland
e-mail: andrea.lovera@femtoprint.ch

David Lambelet
Galatea-Lab,
École Polytechnique Fédérale de Lausanne,
Neuchâtel 2000, Switzerland
e-mail: david.lambelet@epfl.ch

Ilan Vardi
Instant-Lab,
École Polytechnique Fédérale de Lausanne,
Neuchâtel 2000, Switzerland
e-mail: ilan.vardi@epfl.ch

Thomas J. Wolfensberger
Department of Ophthalmology,
University of Lausanne,
Hôpital Ophtalmique Jules-Gonin,
Lausanne 1004, Switzerland
e-mail: thomas.wolfensberger@fa2.ch

Charles Baur
Instant-Lab,
École Polytechnique Fédérale de Lausanne,
Neuchâtel 2000, Switzerland
e-mail: charles.baur@epfl.ch

Simon Henein
Instant-Lab,
École Polytechnique Fédérale de Lausanne,
Neuchâtel 2000, Switzerland
e-mail: simon.henein@epfl.ch

Programmable Multistable Mechanisms for Safe Surgical Puncturing

We present novel medical devices for safe surgical puncturing, in particular a cannula for the treatment of retinal vein occlusion (RVO). This passive mechanical device has an adjustable stroke and exerts a puncturing force independent of operator applied displacement. The innovative feature of this tool is that puncturing stroke is decoupled from operator input thereby minimizing the possibility of overpuncturing. This is achieved using our concept of stability programming, where the user modifies the mechanism strain energy as opposed to imposing direct displacement which is the case for standard bistable mechanisms. Ultra-fast laser three-dimensional (3D) printing is used to manufacture the needle in glass. A microfluidic channel is integrated into the needle tip for drug injection. Numerical simulations and experimental measurements validate the mechanical stability behavior of the puncture mechanism and characterize its puncturing stroke and force. [DOI: 10.1115/1.4043016]

1 Introduction

1.1 Puncturing Problem. Human body puncturing is a common surgical process having associated risks, namely *overpuncturing* where the puncture tool overshoots its target. The tool becomes ineffective and bleeding or even death may occur. A survey of the impact of overpuncturing is given in Ref. [1].

For the purpose of this paper, *puncturing* means entering a region surrounded by a boundary having a higher penetration resistance. Overpuncturing typically occurs because the force used to cross the boundary accelerates the puncturing device and the resulting speed in the low resistance region makes it overshoot the intended target. The challenge, therefore, is to limit the stroke of the puncturing device.

The stroke of the puncture device can be decomposed into surgeon displacement and tool displacement that is displacement of tool moving parts. Surgeon displacement relies on the human capacity to exert a sufficient puncturing force followed by limiting

[1]Corresponding author.
Manuscript received August 10, 2018; final manuscript received February 26, 2019; published online March 21, 2019. Assoc. Editor: Carl Nelson.

the stroke. For delicate operations, human performance may not be sufficiently reliable.

Standard puncturing devices such as trocars have no moving parts, so force and stroke depend on human performance. As explained earlier, an overly large stroke occurs when there is a large puncturing force, so trocars have a sharp bladed tip to reduce puncturing force. However, this increases the consequences of the overpuncturing [2]. The current research is examining robotic surgery which eliminates tremor and limits stroke [3–5].

Another approach is to integrate movable parts into the tool. These tools can be classified into two groups. The first consists of retractable devices where the puncturing tip retracts once puncturing occurs [6,7]. These have proven difficult to scale down to satisfy microsurgical requirements. The second group consists of limited stroke devices [8]. This type of devices will be the subject of this paper. We will show that this technique can be adapted to microsurgery, in particular retinal vein cannulation (RVC).

1.2 Retinal Vein Cannulation. Vein cannulation is an example of delicate micropuncturing. It further requires drug injection so classical trocars cannot be used. A needle punctures the vein and halts inside for the injection duration. In this case, overpuncturing leads to incorrect injection as illustrated in Fig. 1. Cannulation becomes more difficult with decreasing vein size as puncturing force approaches the limits of human performance. One of the most challenging cases is eye surgery.

Retinal vein occlusion (RVO) is an eye condition at which the retinal vein is blocked, resulting in bleeding and reducing oxygen delivery to the retina [9]. This can lead to macular edema, retinal cells death, and neovascularization, all resulting in vision loss [10]. RVO affects 16×10^6 worldwide with more prevalence among the elderly [9].

Retinal vein cannulation is a delicate treatment of RVO [10] and has been proven to be effective. It consists of the following steps, as illustrated in Fig. 2:

(1) The needle contacts the vein.
(2) The needle punctures the vein and halts.
(3) Injection is made.
(4) The needle is retracted.

An intraocular fiber-optic illumination is used to provide visual feedback to the surgeon. It informs the surgeon of puncturing occurrence and drug injection.

Remark. In the case of veins, overpuncturing means puncturing the opposite wall of the vein, so increasing the puncturing angle reduces the possibility of overpuncturing, see Fig. 1.

1.3 Challenges of Retinal Vein Cannulation. Technical difficulties of RVC include the following:

(1) The diameter of the needle tip must be less than the retinal vein diameter which can vary from 50 to 400 μm.

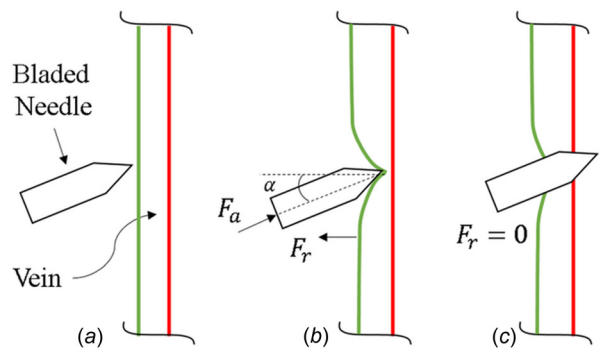

Fig. 1 Vein overpuncturing: F_a and F_r represent the applied and resistance force, respectively and α is the puncturing angle: (*a*) prepuncturing, (*b*) puncturing, and (*c*) overpuncturing

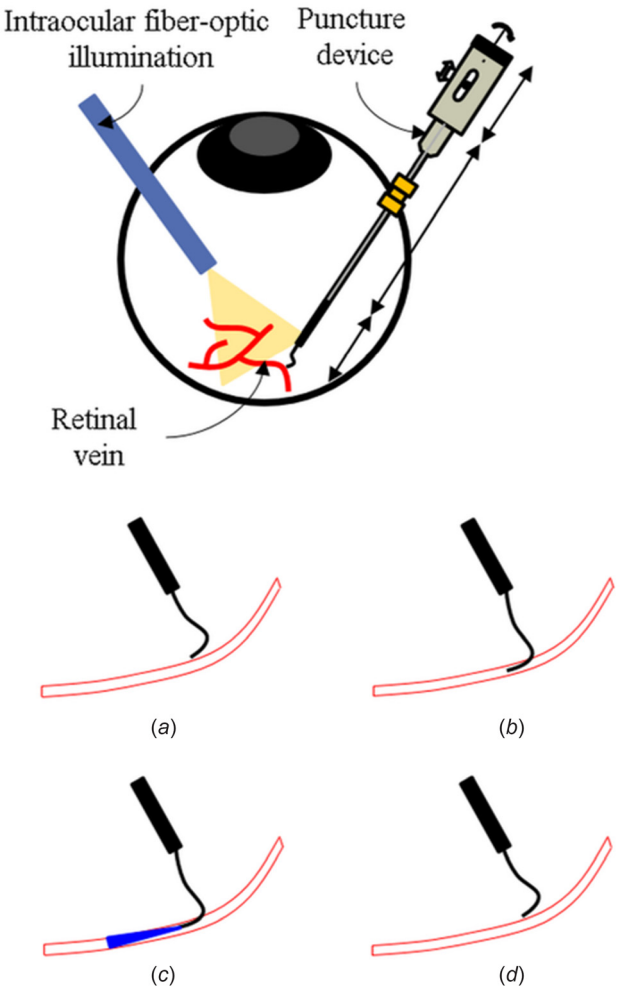

Fig. 2 Retinal vein cannulation: (*a*) needle in contact with the vein, (*b*) needle punctures the vein, (*c*) injection is made, and (*d*) needle retracts from the vein

(2) The needle should be sufficiently sturdy to handle the puncturing process.
(3) Safe puncturing force can be less than 50 mN, beyond human sensing capability. This can require a force sensor.
(4) A gradual force increase can displace the vein instead of puncturing it.
(5) Human tremor is of the order of 100 μm, possibly greater than vein diameter.
(6) The tool should maintain its position during injection which may exceed 10 min.
(7) The entire RVC device should fit into a cylinder of 0.9 mm diameter (20 gage).

Glass micropipettes with sharp tips are commonly used [11], but they can fracture during puncturing. Stainless steel needles with a curved tip have been used [3], but they do not fit in a 20 gage cylinder. Prebent flexible stainless needles have been proposed [4], but they require extra steps to cannulate the vein. A snake-like cannula is presented in Ref. [12], however, it requires precise nanoscale motors for controlling the cannula position.

2 Safe Puncture Optimized Tool for Retinal Vein Cannulation

The main result of this paper is a new passive mechanical puncture tool, the safe puncture optimized tool (SPOT). Compliant micromechanisms are integrated within the cannula to limit its stroke independent of surgeon displacement. The main novelty is

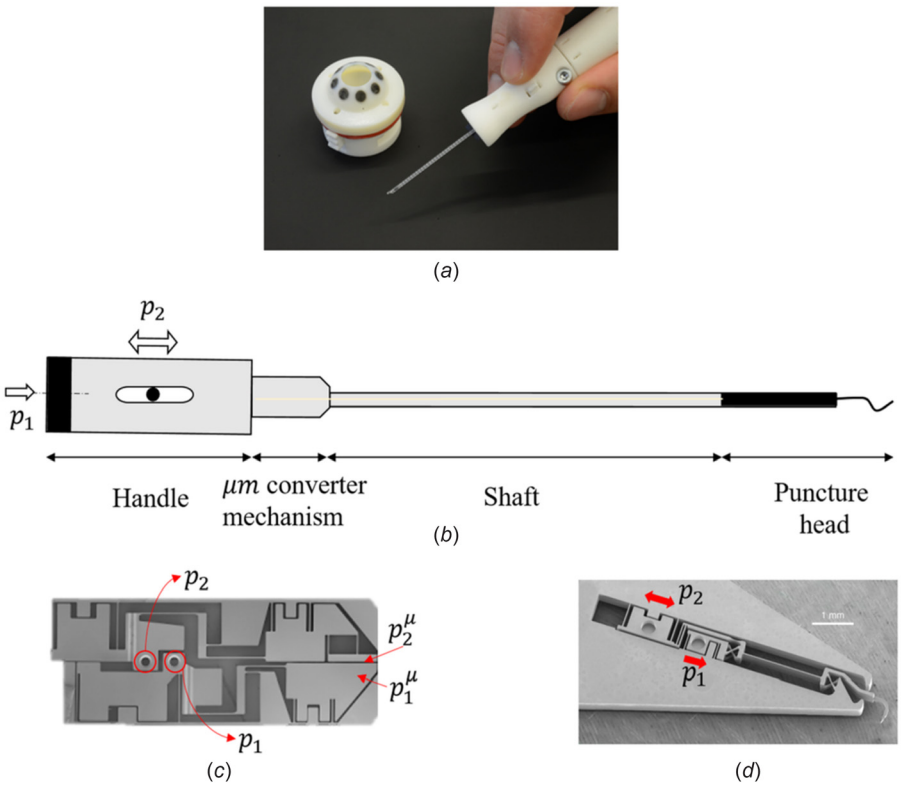

Fig. 3 (*a*) Our tool, (*b*) graphical representation, (*c*) microconverter mechanism, and (*d*) puncture mechanism

the application of *stability programming*, a concept introduced in our previous work [13]. This allows the stroke of the tool to be adjusted mechanically to a fixed value and be decoupled of the operator displacement.

Figure 3 gives the main components of the puncture tool including handle, shaft, and puncture mechanism. The handle has two inputs at which the surgeon applies p_1^a and p_2^a. These inputs are converted to microscale as, p_1 and p_2, and transferred to the puncture mechanism via shafts. The input p_1 adjusts the tool stroke based on the vein diameter and p_2 triggers the puncturing.

The puncture mechanism has two stable states, prepuncturing and postpuncturing states, given in Figs. 4(*a*) and 4(*b*), respectively. At $p_2 = p_2^r$, the mechanism switches from the prepuncture to the postpuncture state and puncturing occurs. In this paper, we focus only on the design of the puncture mechanism given in Fig. 3(*d*).

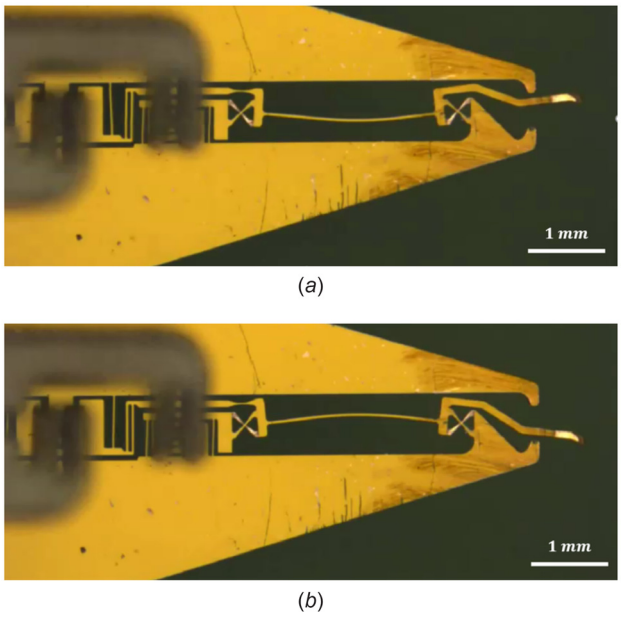

Fig. 4 Stable states of the mechanism for $p_1 = 10$ μm, puncturing occurs on switching from (*a*) prepuncturing state to (*b*) postpuncturing state

2.1 Utilization Protocol. The surgeon uses the following protocol to cannulate the retinal vein using a visual feedback from the microscope:

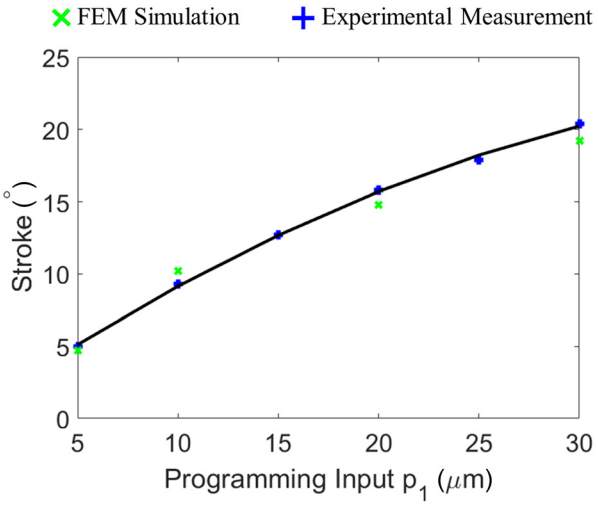

Fig. 5 The angular stroke of the needle tip versus p_1 based on numerical and experimental measurements

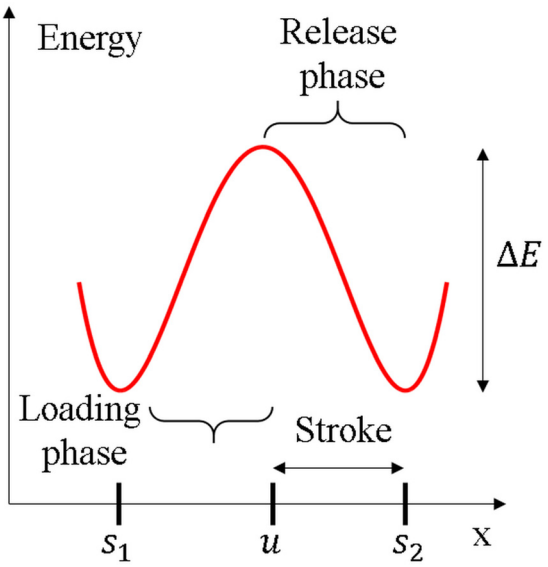

Fig. 6 Strain energy of displacement-driven bistable mechanism as a function of its position *x*

(1) The value of p_1 determines the stroke which is adjusted by rotating a disk, see Fig. 3.
(2) The surgeon selects an initial value $p_1 = p_1^d$ based on the vein diameter, so that the tool will not overpuncture, see Fig. 5.
(3) The tool is initially at its prepuncturing state.
(4) The surgeon uses optical feedback to place the tool tip in contact with the vein.
(5) In order to change the puncturing state, the surgeon modifies p_2 using a slider on the tool handle, see Fig. 3.
(6) The surgeon pushes the p_2 slider until visual feedback indicates that the tool is at its postpuncturing state.
(7) Using visual feedback, the surgeon determines if puncturing has occurred.
(7a) If puncturing occurs without overpuncturing, the procedure is successful.
(7b) If overpuncturing has occurred, then the procedure has failed.
(7c) If puncturing has not occurred, the surgeon pulls the p_2 slider till the tool reaches its prepuncturing state, the surgeon slightly increases p_1 and returns to step 6.

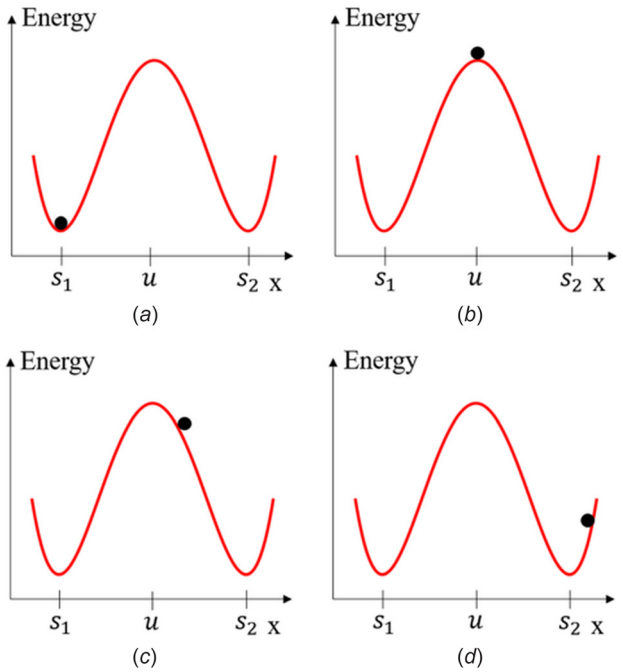

Fig. 7 Strain energy of displacement-driven bistable mechanism where the mechanism position is denoted by the ball at (*a*) stable state s_1, (*b*) unstable state u (*c*) overload $x_u > 0$, and (*d*) surpassing of s_2 depends on overload x_u

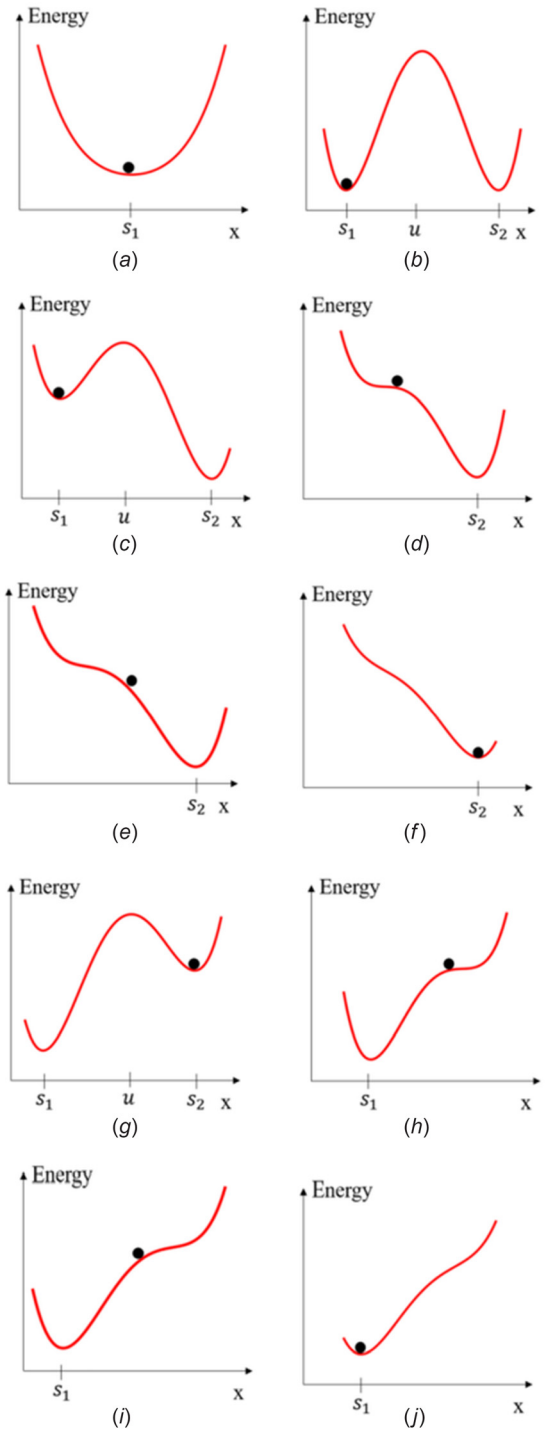

Fig. 8 Strain energy of programmable bistable mechanism for different values of p_1 and p_2: (*a*) $p_1 < p_1^{cr}$, (*b*) $p_1 > p_1^{cr}$, $p_2 = 0$, (*c*) $p_1 > p_1^{cr}$, $0 < p_2 < p_2^s$, (*d*) $p_1 > p_1^{cr}$, $p_2 = p_2^s$, (*e*) $p_1 > p_1^{cr}$, $p_2 = p_2^r$, (*f*) $p_1 > p_1^{cr}$, $p_2 > p_2^r$, (*g*) $p_1 > p_1^{cr}$, $-p_2^s < p_2 < 0$, (*h*) $p_1 > p_1^{cr}$, $p_2^s < p_2 < 0$, (*i*) $p_1 > p_1^{cr}$, $p_2 = -p_2^r$, and (*j*) $p_1 > p_1^{cr}$, $p_2 < -p_2^r$

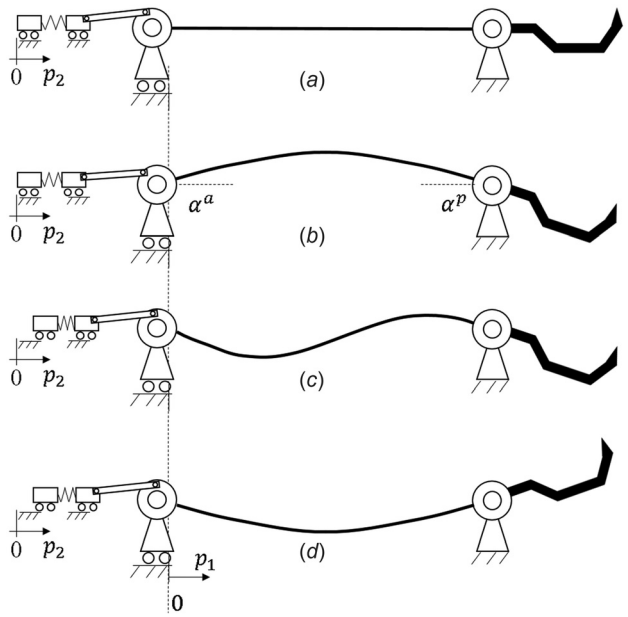

Fig. 9 Mechanism deformation for (*a*) initial state, (*b*) prepuncturing state, (*c*) unstable state, and (*d*) postpuncturing state

In the case of successful puncturing, the cannulation is continued by drug injection. Following injection, the surgeon pulls the p_2 slider returning the tool to its prepuncturing state and removes the tool from the eye.

2.2 Theoretical Design

2.2.1 Mechanical Multistability. Our tool relies on the concept of multistability to produce repeatable puncturing with tunable stroke. Multistable mechanisms are mechanical devices which have more than one stable state within their range of motion [14]. They store and release strain energy as they deform under imposed displacement x or force F. They can function as switch when displaced between their stable states and characterized by their rapid energy release once they surpass their unstable state. A simple example is the bistable mechanism as realized by a hair clip.

Multistable mechanisms are used to improve the safety of medical operations such cranial drilling as they rapidly release energy on surpassing their unstable state. This was utilized to prevent overdrilling [7].

2.2.2 Definitions. The strain energy of multistable mechanisms has N energy minima corresponding to *stable states*, $s_1, s_2, \ldots, s_N$ and $N-1$ energy maxima representing *unstable states*, $u_1, u_2, \ldots, u_{N-1}$, as illustrated in the strain energy in Fig. 6(*a*), where $N=2$. Energy is required to surpass the *barrier* (ΔE) existing between the stable states.

We distinguish two categories of multistable mechanisms based on the actuation method, the first category is *displacement-driven multistable mechanisms* in which the position is altered without modifying the energy profile and *programmable multistable mechanisms* in which the energy profile is modified by the displacement imposed.

2.2.3 Displacement-Driven Bistable Mechanism. One degree-of-freedom (DOF) bistable mechanisms can be displaced between their stable states by imposing direct displacement to modify their position x, as illustrated in Fig. 6. As x increases from stable state s_1, the stored strain energy increases until the mechanism reaches its unstable state u, we call this the *loading phase*. After that, the mechanism releases its stored energy till it reaches its other stable state s_2, we call this the *release phase*. Since the energy profile is fixed, the exerted force during the release phase is repeatable for the given stroke, as illustrated by the reaction force in Fig. 6.

In order to reach the release phase, the operator must displace the mechanism up to a displacement $x_u > u$, we call this *overloading*. At overloading, the operator applies a force thereby adding energy to the system which increases the stroke. This means that repeatability of the energy release depends on the repeatability of x_u, which is difficult if $x_u - u$ is of the order of human sensory perception. Figure 7 illustrates the impact of overload on the mechanism position where the ball represents the mechanism state.

For human-driven microscale devices, displacement-driven multistable mechanisms do not have a high degree of repeatable energy release and stroke. Therefore, imposed displacement and

Fig. 11 A 3D cross pivot for beam anchoring

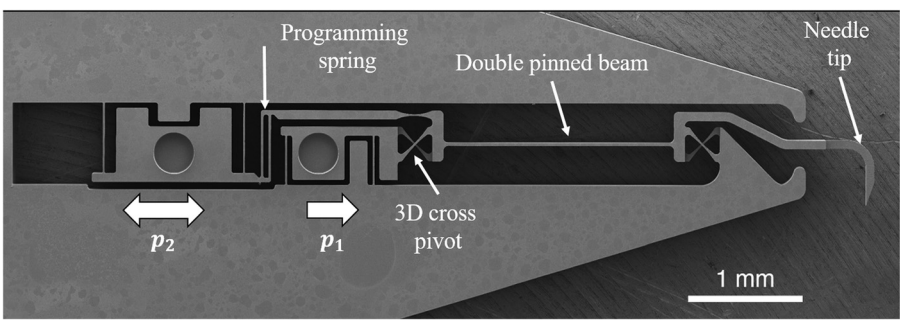

Fig. 10 The puncture mechanism illustrating its main components and the programming inputs, p_1 and p_2

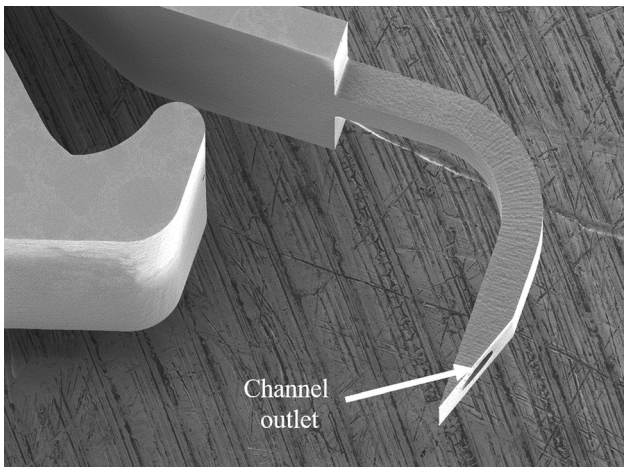

Fig. 12 The needle tip with an integrated fluidic channel for drug injection

the mechanism position should be decoupled; this can be implemented by programmable multistable mechanisms.

2.2.4 Programmable Multistable Mechanism. Programmable multistable mechanisms have an energy profile modified by external inputs that we call *programming inputs*. These inputs can change the number and position of stable states as well as trigger energy release. In this paper, we consider only the case of stability programming between monostability and bistability.

Figure 8 gives the strain energy of the programmable multistable mechanism used in our tool. We describe the energy profiles corresponding to the protocol steps given in Sec. 2.1. Once again, the ball represents the state.

Initially, the mechanism is monostable as given in Fig. 8(*a*) corresponding to Step 1. As p_1 is increased, the mechanism becomes bistable and the stroke is tuned by selecting $p_1 = p_1^d$ of Step 2, as illustrated in Fig. 8(*b*). The mechanism is in state s_1.

Step 6 corresponds to Figs. 8(*c*)–8(*f*). As p_2 is increased, the energy profile remains bistable until $p_2 = p_2^s$ as shown in Fig. 8(*c*). The mechanism remains in state s_1 during this step (the variation of s_1 with respect to p_2 is negligible).

At p_2^s, the mechanism is once again monostable with stable state s_2, as illustrated in Fig. 8(*d*). As p_2 is further increased, there is a value p_2^r at which the mechanism overcomes static damping and starts to release energy, see Fig. 8(*e*).

Energy release rapidly displaces the mechanism to state s_2 independent of p_2 overload as shown in Fig. 8(*f*). Further increase of p_2 slightly affects the position of the mechanism.

Step 7c corresponds to Figs. 8(*g*)–8(*i*), simply reversing the steps illustrated in Figs. 8(*c*)–8(*e*) by decreasing p_2.

Key remark. Figure 8(*e*) always occurs at the same value p_2^r, so energy release is repeatable and stroke is decoupled from operator actuation input.

2.3 Tool Design. We chose a programmable multistable mechanism having the energy profiles in Fig. 8. The conceptual design is shown in Fig. 9 and our physical construction satisfies the requirements of retinal vein cannulation discussed in Sec. 1.3.

2.3.1 A Conceptual Design. A conceptual representation of our tool is given in Fig. 9, it consists of a beam anchored on both sides via pivots. The *puncturing pivot* is connected to the needle tip and fixed to the tool frame. The body of the *actuation pivot* translates according to p_1 in the axial direction of the beam.

The input p_2 acts by translating a slider which loads a *programming spring* translating an intermediate block which in turn rotates the actuation pivot via a rigid link. The angular position α^a of the

Fig. 13 Three-dimensional rendering of the deformation of the puncture mechanism based on finite element model (FEM) simulations

actuation pivot determined by p_2 leads to an angular deflection α^p of the puncturing pivot.

When $p_1 = 0$, the beam is straight so $\alpha^a = \alpha^p = 0$. As p_1 increases, it remains straight until $p_1 > p_1^{cr}$ when the beam buckles. Further increase of p_1 increases the strain energy and leads to higher energy release. A suitable value is chosen, e.g., p_1^d, as discussed in Sec. 2.1.

The buckled beam has two stable states corresponding to the prepuncturing and postpuncturing states, having angular deflections α_1^a, α_1^p and α_2^a, α_2^p, respectively.

Starting at the prepuncturing state, α_1^a, α_1^p, puncturing occurs by increasing p_2 which rotates the actuation pivot clockwise. The mechanics of the double pinned buckled beam is such that the puncture pivot rotates imperceptibly, so that α^p has essentially the same value α_1^p [15]. On reaching p_2^r of Sec. 2.2.4, the mechanism releases its energy and rapidly reaches its postpuncturing state and α_1^p switches to α_2^p, this corresponds to the puncturing phase.

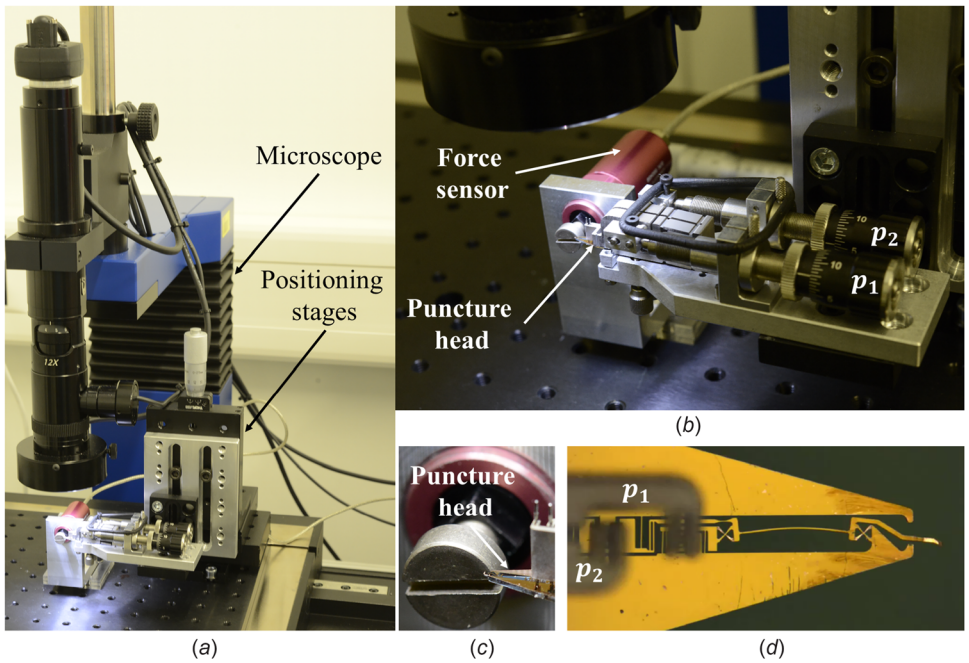

Fig. 14 (*a*) Experimental setup, (*b*) driving micrometric screws and force sensor, (*c*) interface between the sensor and the needle tip, and (*d*) the puncture mechanism under microscope

2.3.2 Flexure-Based Realization. The equivalent flexure mechanism of our conceptual design is given in Fig. 10. It consists of a beam anchored on both extremities by three-dimensional (3D) cross pivots corresponding to the double pinned beam. Each pivot has three overlapped beams with optimized profile to increase their stroke as illustrated in Fig. 11. The needle tip is connected to the puncture pivot and contains a fluidic channel for drug injection as shown in Fig. 12.

The actuation pivot is guided by a parallel beam stage at which p_1 is imposed. The input p_2 is applied on a parallel beam stage which is connected serially to the programming spring which consists of two beams. The programming spring is serially connected to the actuation pivot via a circular hinge. Stoppers are used to limit the range of p_1 and p_2 and puncture angle α_p.

2.3.3 Tool Advantages. Our mechanism has the following advantages for retinal vein cannulation:

(1) Multistable mechanisms release their energy rapidly, thereby addressing standard cannulation problems (Sec. 1.3).
(2) The stroke of the tool is independent of surgeon actuation during puncturing, thereby decreasing the possibility of overpuncturing (Sec. 2.2.4).
(3) Tool stroke can be adjusted by the surgeon prior to puncturing making the tool adaptable to different vein sizes. Moreover, this allows gradual stroke increase for a given vein, thereby minimizing the possibility of overpuncturing (Sec. 2.1).
(4) The needle tip has nonsignificant movement during the loading phase, thereby decreasing the variability of the tool positioning (Sec. 2.2).
(5) The maximum force exerted by the tool is adjustable, thereby eliminating the need for a force sensor (Sec. 1.3).
(6) Once inside the vein, the needle position is stable making this suitable for long injection periods exceeding 10 min (Sec. 1.3).

3 Dimensioning

We used the finite element method to dimension the mechanism. COMSOL solid mechanics module was selected to calculate the mechanism strain energy in terms of programming inputs, thereby estimating the tool stroke. Mesh convergence tests were performed to ensure solution validity.

The mechanism dimensions were selected to satisfy the specifications of Sec. 1.3: a programmable stroke from 5 deg to 20 deg and a puncturing force exceeding 8 mN.

Our FEM simulations showed that these specifications are satisfied when the double pinned beam has length 2 mm, thickness 30 μm, width 200 μm and the programming spring consists of two identical beams, each of length 500 μm and thickness 25 μm. Figure 13 illustrates the mechanism deformation for the selected dimensions, based on FEM.

4 Fabrication

We used fused silica (glass) as our tool material since its elastic properties are consistent with the tool specifications. A femtolaser modifies fused silica whose transparency at the selected wavelength allows laser penetration. The laser is absorbed where focused changing the material properties, in particular, the etching rate, which is 200 times higher in exposed regions than in unexposed regions. Accordingly, the tool dimensions were adapted to different etching rates. This allowed us to satisfy the tight fabrication tolerances, which are of order 1 μm.

We exposed a 500 μm thick fused silica to a 1030 nm femtosecond laser focused by a 20*X* objective 0.4 numerical aperture lens. Exposure took 30 min and the etching lasted 8 h. The tool was manufactured in collaboration with FEMTOprint SA using their innovative technology [16–18].

5 Characterization

The mechanical behavior of the puncture tool is studied including the mechanism stroke, puncturing force, number of stable states, and their positions. An experimental setup is built to verify the mechanical behavior of the tool. The tool functionality was tested by the cannulation of the retinal vein of pig eyes.

5.1 Experimental Measurements. We validate numerically and experimentally the stability behavior of the tool, i.e., we evaluate the number and positions of the stable states for given programming inputs. Then, we study the effect of the programming

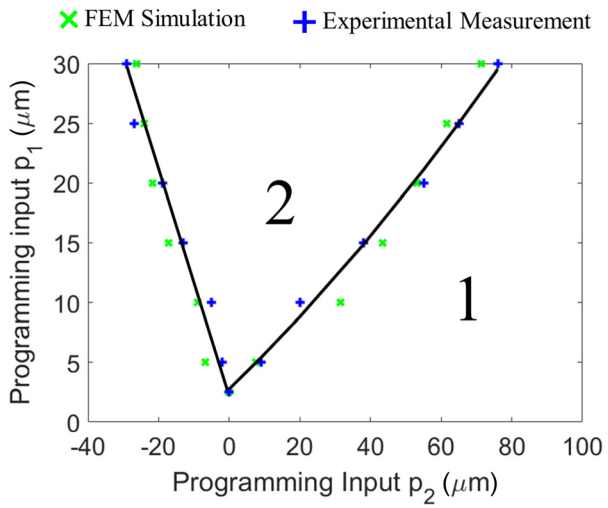

Fig. 15 Programming diagram giving the relation between the number of stable states and programming inputs

inputs on the mechanism stroke and puncture force, the crucial parameters for successful puncturing.

An experimental setup was built to characterize the mechanical behavior of the puncture tool. The spatial position of the puncture tool was controlled by a 5DOF stage as illustrated in Fig. 14. Programming inputs were applied by micrometric screws and their values were measured using an optical microscope of resolution 0.5 μm. A Futek LPM 200 load cell with resolution of 0.1 mN was used to measure puncturing force of the needle tip.

5.2 Results and Discussion. The number of stable states as a function of the programming inputs is illustrated by the *programming diagram*, as shown in Fig. 15. This characterizes the qualitative behavior of the mechanism.

The set of values (p_1, p_2) is divided into regions where the mechanism is monostable versus bistable. As explained in Sec. 2.2, the boundaries between these regions correspond to p_2^r which depends on p_1.

We also explicitly computed and experimentally validated the energy profiles for given values (p_1, p_2). In particular, Fig. 16 shows how for $p_1 = 15$ μm, the energy profile changes for a given set of p_2 values. This corresponds to puncturing as explained in Sec. 2.2. It is seen that the qualitative nature of energy profile is consistent with the discussion of Sec. 2.2.

An advantage of our tool is decoupling the surgeon actuation input p_2 and the puncture pivot position α^p before and after energy release as illustrated in Fig. 17 for $p_1 = 15$ μm. As p_2 changes, α^p is slightly modified. At $p_2 = p_2^r$, the mechanism snaps to its postpuncturing state. The value at which the mechanism switches between its stable states depends on the direction of the applied p_2.

We validated the ability to tune stroke using p_1. Figure 5 illustrates the relation between the stroke and p_1. This shows that the stroke increases with p_1 ensuring that a significant range of strokes is possible making the tool adaptable to different vein diameters. In addition, Fig. 18 shows that the maximum force at the needle tip increases with increasing p_1 where quasi-static measurement conditions are applied.

5.3 Pig Eye Testing. We used pig eyes to verify the functionality of the tool. The retinal vein of pig eyes was successfully

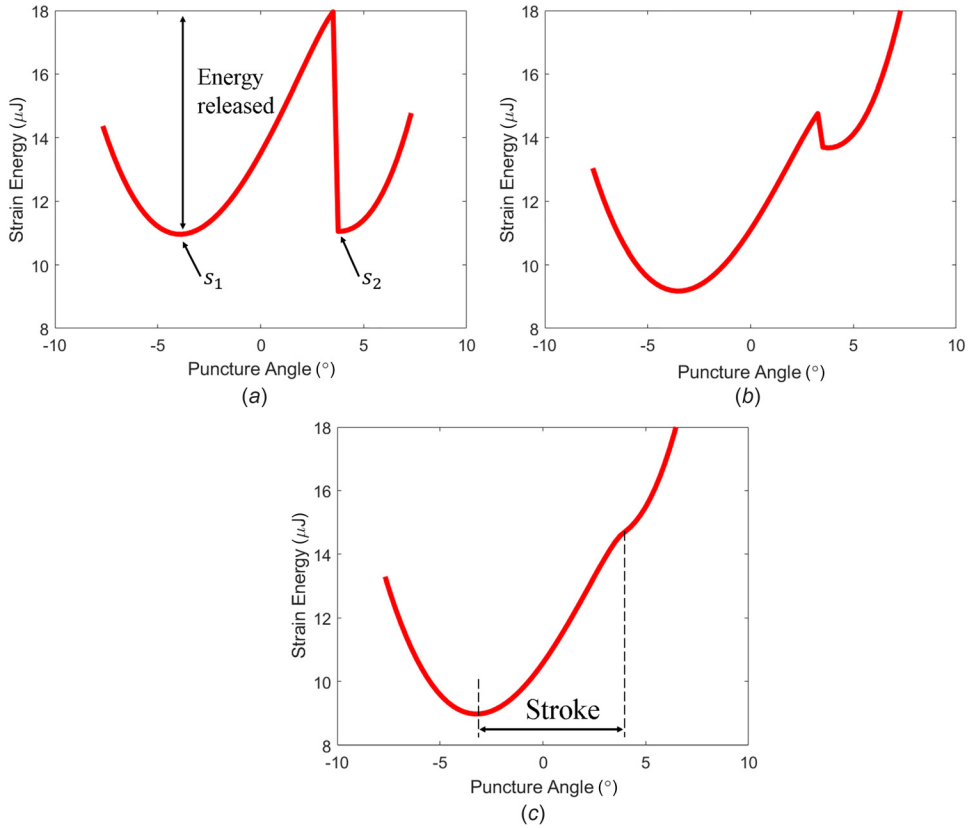

Fig. 16 Strain energy of the puncture mechanism for $p_1 = 15$ μm on switching from prepuncturing state s_1 to postpuncturing state s_2 based on FEM simulations on increasing p_2: (*a*) the mechanism is bistable with stable states, s_1, s_2, (*b*) the energy barrier decreases on increasing p_2, and (*c*) the mechanisms is monostable and the prepuncturing state vanishes

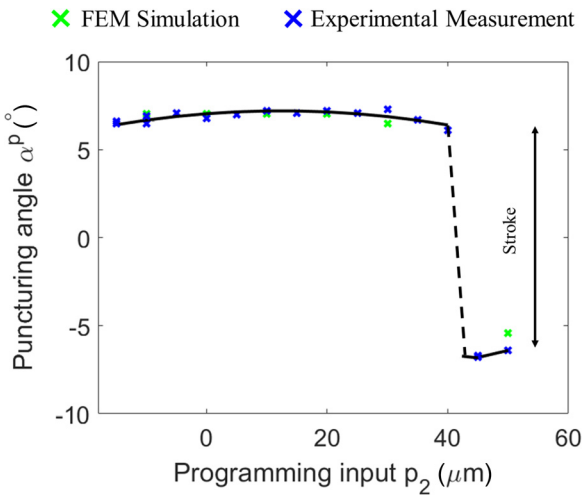

Fig. 17 The angular position of the needle tip as a function of p_2 at $p_1 = 15$ μm based on numerical and experimental measurements

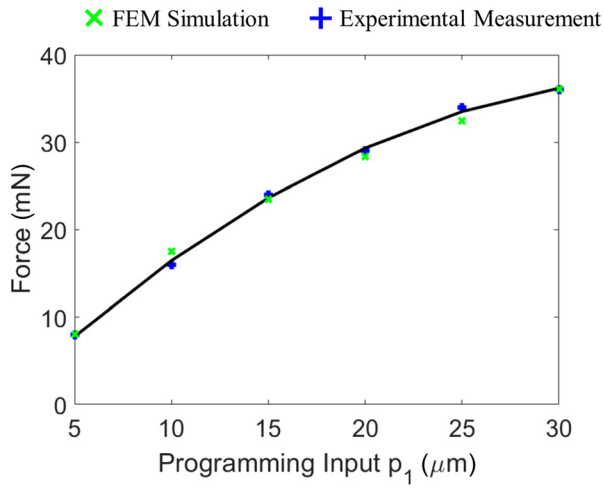

Fig. 18 The maximum force during energy release in quasi-static mode versus p_1 based on numerical and experimental measurements

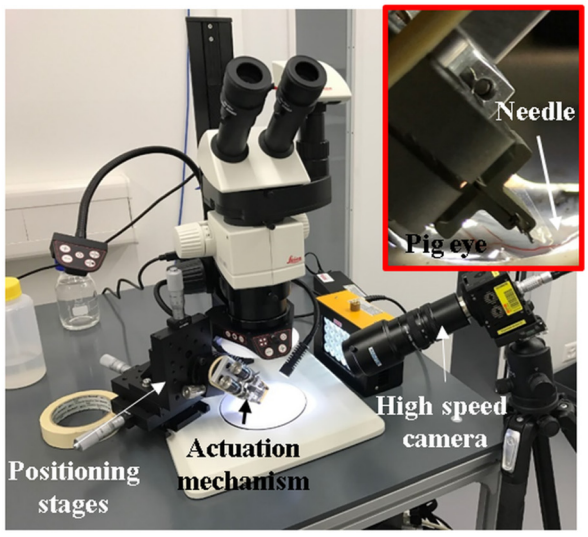

(*a*)

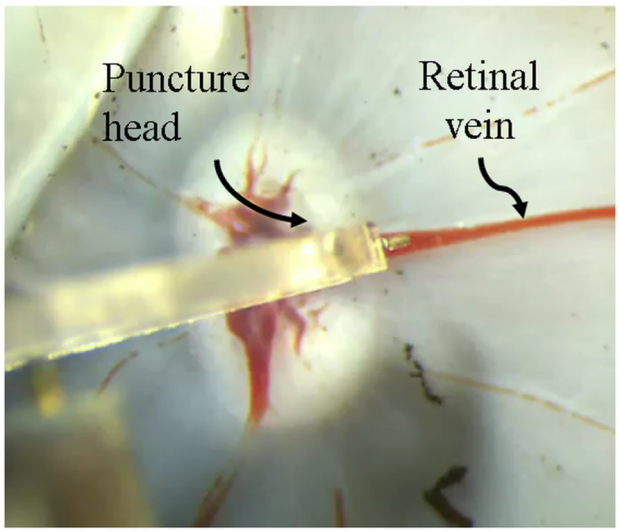

(*b*)

Fig. 19 (*a*) Pig eye cannulation setup and (*b*) puncture mechanism in contact with the retinal vein

cannulated. We used optical microscope and high speed camera to verify the vein cannulation as illustrated in Fig. 19.

The pig eyes were prepared as follows: we split the eye into two parts so that the retina is easily accessed without being deformed. Second, we removed the vitreous humor by capillary forces so we can verify the puncturing occurrence. After that, the puncture tool was positioned using the 5DOF stage so that the needle is in contact with the vein at its prepuncturing state. Micrometric screws were used to program and trigger the puncturing. A Leica M125 stereo microscope is used to assess the needle tip position.

The minimum vein diameter successfully cannulated is 150 μm. This limitation is returned to the accuracy of the positioning stage and vein motion during the tool loading phase of the tool.

6 Conclusion and Perspectives

We applied our concept of stability programming [13] to design retinal vein cannulas for the treatment of vein occlusion. Our theoretical analysis indicates that stability programming can advantageously decouple operator input from instrument position enabling safe puncturing. This was further verified by experimental measurements.

On the manufacturing side, our constructed tool is one of the first examples of complicated 3D structures manufactured by ultra-fast laser printing in glass highlighting the great potential of this technology.

Our current research focuses on adapting the tool to other medical microsurgeries requiring delicate procedures.

Acknowledgment

This work was funded by the Swiss commission of technology and innovation (CTI), rebranded as Innosuisse, FEMTOprint SA, and Jules Gonin Hospital. We acknowledge technical discussions and collaboration with Galatea Lab, in particular, Professor Yves Bellouard and Sacha Pollonghini. We as well thank Nicolas Ferrier and Sebastian Fifanski for their help on experimental measurements.

References

[1] Krishnakumar, S., and Tambe, P., 2009, "Entry Complications in Laparoscopic Surgery," J. Gynecol. Endoscopy Surg., **1**(1), pp. 4–11.

[2] Fanning, J., Shah, M., and Fenton, B., 2011, "Reduced-Force Closed Trocar Entry Technique: Analysis of Trocar Insertion Force Using a Mechanical Force Gauge," J. Soc. Laparoendoscopic Surg., **15**(1), pp. 59–61.
[3] Gijbels, A., Vander Poorten, E. B., Stalmans, P., and Reynaerts, D., 2015, "Development and Experimental Validation of a Force Sensing Needle for Robotically Assisted Retinal Vein Cannulations," IEEE International Conference on Robotics and Automation (ICRA), Seattle, WA, May 26–30, pp. 2270–2276.
[4] Gonenc, B., Tran, N., Gehlbach, P., Taylor, R. H., and Iordachita, I., 2016, "Robot-Assisted Retinal Vein Cannulation With Force-Based Puncture Detection: Micron vs. the Steady-Hand Eye Robot," IEEE Annual International Conference of the Engineering in Medicine and Biology Society (EMBC), Orlando, FL, Aug. 16–20, pp. 5107–5111.
[5] Yu, H., Shen, J.-H., Joos, K. M., and Simaan, N., 2013, "Design, Calibration and Preliminary Testing of a Robotic Telemanipulator for Oct Guided Retinal Surgery," IEEE International Conference on Robotics and Automation (ICRA), Karlsruhe, Germany, May 6–10, pp. 225–231.
[6] Begg, N., 2014, "A Novel Tip-Retraction Mechanism for Puncture Devices," ASME J. Mech. Des., **136**(10), p. 105002.
[7] Loschak, P. M., Xiao, K., Pei, H., Kesner, S. B., Thomas, A. J., and Walsh, C. J., 2013, "Assured Safety Drill With Bi-Stable Bit Retraction Mechanism," ASME Paper No. DETC2013-12088.
[8] Wyrick, R. E., 2007, "Medicine Injection Devices and Methods," U.S. Patent No. 7,297,136.
[9] Rogers, S., McIntosh, R. L., Cheung, N., Lim, L., Wang, J. J., Mitchell, P., Kowalski, J. W., Nguyen, H., and Wong, T. Y., 2010, "The Prevalence of Retinal Vein Occlusion: Pooled Data From Population Studies From the United States, Europe, Asia, and Australia," Ophthalmology, **117**(2), pp. 313–319.
[10] Wong, T. Y., and Scott, I. U., 2010, "Retinal-Vein Occlusion," New Engl. J. Med., **363**(22), pp. 2135–2144.
[11] Asami, T., Kaneko, H., Miyake, K., Ota, I., Miyake, G., Kato, S., Yasuda, S., Iwase, T., Ito, Y., and Terasaki, H., 2016, "An Endovascular Cannulation Needle With an Internal Wire for the Fragmentation of Thrombi in Retinal Vein Occlusion," Transl. Vision Sci. Technol., **5**(5), p. 9.
[12] He, X., Van Geirt, V., Gehlbach, P., Taylor, R., and Iordachita, I., 2015, "IRIS: Integrated Robotic Intraocular Snake," IEEE International Conference on Robotics and Automation (ICRA), Seattle, WA, May 26–30, pp. 1764–1769.
[13] Zanaty, M., Vardi, I., and Henein, S., 2018, "Programmable Multistable Mechanisms: Synthesis and Modeling," ASME J. Mech. Des., **140**(4), p. 042301.
[14] Henein, S., 2001, *Conception Des Guidages Flexibles*, PPUR Presses Polytechniques, Lausanne, Switzerland.
[15] Dehon, N., 2012, Escapement Mechanism, U.S. Patent No. 8,303,167.
[16] Steimle, A., 2018, "3D Micro-Printing: A New Era for Med-Tech Applications," Laser Tech. J., **15**(1), pp. 32–34.
[17] Bellouard, Y., Said, A., Dugan, M., and Bado, P., 2004, "Fabrication of High-Aspect Ratio, Micro-Fluidic Channels and Tunnels Using Femtosecond Laser Pulses and Chemical Etching," Opt. Express, **12**(10), pp. 2120–2129.
[18] FEMTOprint, 2018, "FEMTOprint SA," Femtoprint, Muzzano, Switzerland, accessed Apr. 2, 2018, www.femtoprint.ch/